Inorganic Chemistry

Article

pubs.acs.org/IC

The Effect of Ligand Lipophilicity on the Nanoparticle Encapsulation of Pt(IV) Prodrugs

Timothy C. Johnstone and Stephen J. Lippard*

Department of Chemistry, Massachusetts Institute of Technology, Cambridge, Massachusetts 02139, United States

Supporting Information

ABSTRACT: In an effort to expand the therapeutic range of platinum anticancer agents, several new approaches to platinum-based therapy, including nanodelivery, are under active investigation. To better understand the effect of ligand lipophilicity on the encapsulation of Pt(IV) prodrugs within polymer nanoparticles, the series of compounds *cis,cis,trans*-[Pt-$(NH_3)_2Cl_2L_2$] was prepared, where L = acetate, propanoate, butanoate, pentanoate, hexanoate, heptanoate, octanoate, nonanoate, and decanoate. The lipophilicities of these compounds, assessed by reversed-phase HPLC, correlate with the octanol/water partition coefficients of their respective free carboxylic acid ligands, which in turn affect the degree of encapsulation of the Pt(IV) complex within the hydrophobic core of poly(lactic-*co*-glycolic acid)-*block*-poly(ethylene glycol) (PLGA-PEG-COOH) nanoparticles. The most lipophilic compound investigated, *cis,cis,trans*-[$Pt(NH_3)_2Cl_2(O_2C-(CH_2)_8CH_3)_2$], displayed the best encapsulation. This compound was therefore selected to evaluate the effect of increased platinum concentration on encapsulation. As the platinum concentration was increased, there was an initial increase in encapsulation followed by a decrease due to macroscopic precipitation. Maximal loading occurred when the platinum complex was present at a 40% w/w ratio with respect to polymer during the nanoprecipitation step. Particles formed under these optimal conditions had diameters of approximately 50 nm, as determined by transmission electron microscopy.

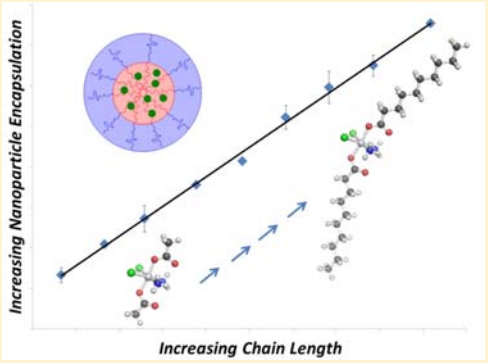

INTRODUCTION

Following the serendipitous discovery of anticancer activity for *cis*-[$Pt(NH_3)_2Cl_2$], or cisplatin,[1] it has come to be one of the most widely used chemotherapeutic agents for the treatment of testicular, ovarian, bladder, and nonsmall cell lung cancers (NSCLC), as well as small cell lung cancer (SCLC), melanoma, lymphomas, and myelomas.[2] The advantages of platinum-based treatment are perhaps most evident in testicular cancer, where, following the introduction of cisplatin into the arsenal of available treatments, cure rates have risen to >90%.[3] Despite the clinical efficacy demonstrated by platinum-based drugs currently approved by the FDA, intense research is underway to discover variants with enhanced efficacy, lower toxicity, and a more diverse spectrum of activity.[4] One approach, which offers several potential advantages, is to use nanosized drug delivery vehicles.[5] The controlled release provided by these systems can enhance retention in the bloodstream, their size allows for passive targeting, and their surfaces can be functionalized for active targeting. With collaborators, our lab has reported the preparation of Pt(IV) constructs designed for delivery by gold nanoparticles,[6] single-walled carbon nanotubes,[7,8] and polymeric nanoparticles.[9−11]

Most platinum complexes investigated for their cytotoxic activity are unsuitable for nanoparticle encapsulation. Different approaches have been used to produce analogues that can be integrated into a nanodelivery device. One strategy that we previously described involved the introduction of the hydrophobic axial ligands L (L = hexanoate) into the coordination sphere of a *cis,cis,trans*-[$Pt(NH_3)_2Cl_2L_2$], platinum(IV) complex, allowing it to be encapsulated within the hydrophobic core of a polymeric micelle.[9] The micelle used in the prior study was composed of carboxy-terminated amphiphilic poly(lactic-*co*-glycolic acid)-*block*-poly(ethylene glycol) (PLGA-PEG-COOH) copolymers, the self-assembly of which has been exploited previously for the construction of other drug delivery vehicles.[12] The hexanoate ligands L of the Pt(IV) complex provided sufficient lipophilicity to promote encapsulation within the PLGA nanoparticle core. The remaining ligands in the coordination sphere are such that, following the reduction of this Pt(IV) complex, an equivalent of cisplatin would be released as the active Pt(II) cytotoxic payload.

These results raised the question, is the addition of two lipophilic carboxylates to a Pt(II) core complex a readily generalizable strategy for nanodelivery of platinum(IV) anticancer prodrugs? Before exploring different Pt(II) core structures, however, we wanted to understand the precise effect of carboxylate ligand choice on the nanoprecipitation process used to form the polymeric micelles. We therefore undertook the present study of a series of compounds of the form

Received: April 29, 2013
Revised: June 13, 2013
Accepted: June 28, 2013
Published: July 16, 2013

   dx.doi.org/10.1021/ic4010642 | Inorg. Chem. 2013, 52, 9915−9920

cis,cis,trans-$[Pt(NH_3)_2Cl_2(OOCR)_2]$, where R is a straight chain alkyl (Scheme 1). The complexes comprising this series all

Scheme 1. Synthesis and General Structure of the Pt(IV) Carboxylate Species Studied

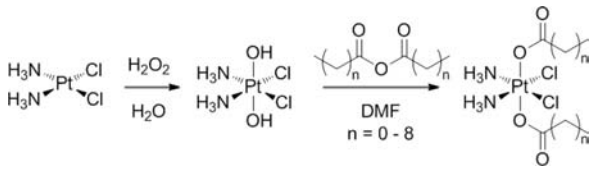

contain a *cis*-diamminedichloroplatinum core as the pharmacophore and two axial ligands that vary systematically in length. In previous related work, a series of Pt(IV) carboxylate complexes containing either a *cis*-1,4-diaminocyclohexanedichloroplatinum[13] or a *trans*-1*R*,2*R*-diaminocyclohexanedichloroplatinum pharmacophore[14] were used to explore the influence of axial ligand chain length on the biological properties of the complex. The aim of the present work, however, is to exploit the axial ligands for nanoparticle encapsulation with the aim of enhancing anticancer efficacy. The efficiency of nanoparticle encapsulation was investigated and correlated with the physical properties of the carboxylate ligands. The effect of relative platinum complex concentration during the nanoprecipitation procedure on the degree of encapsulation was also studied. Two competing processes, nanoparticle encapsulation and bulk precipitation, were correlated with this parameter, and conditions for maximal loading were determined by finding the optimal balance between these two processes.

EXPERIMENTAL SECTION

General Procedures and Chemicals for Synthesis. All chemicals were reagent grade and used as purchased without further purification. Acetic, butanoic, and pentanoic anhydrides were obtained from Sigma-Aldrich. Propanoic, hexanoic, heptanoic, and octanoic anhydrides were purchased from TCI America. Nonanoic and decanoic anhydrides were prepared by the DCC-mediated dehydration of the corresponding carboxylic acids,[15] which were obtained from TCI America. Solvents were used as received without further purification. *cis,cis,trans*-$[Pt(NH_3)_2Cl_2(OH)_2]$, compound **1**, was prepared as previously described.[16] The PLGA-PEG-COOH block copolymer, prepared as described previously,[17] was kindly provided by the Farokhzad Lab (Suresh Gadde, Harvard Medical School). Milli-Q water was used for all work involving nanoparticles.

Physical Measurements. ^1H and $^{13}C\{^1H\}$ NMR measurements were performed on a Varian Inova-500 spectrometer in the MIT Department of Chemistry Instrumentation Facility with deuterated DMSO as a solvent. NMR chemical shifts (δ) are reported in parts per million with respect to tetramethylsilane and referenced to residual solvent peaks. NMR spectra are presented in Supporting Information Figures S1–S18. Fourier-transform infrared spectra were recorded on a ThermoNicolet Avatar 360 spectrophotometer using the *OMNIC* software. All IR samples were prepared as KBr pellets and measurements are reported in cm^{-1}. Electrospray ionization mass spectrometry (ESI-MS) measurements were performed on an Agilent Technologies 1100 series LC/MSD ion trap. Liquid chromatography–mass spectrometry (LC–MS) measurements were performed using the same ion source and trap.

Synthesis. Compounds of the general formula *cis,cis,trans*-$[Pt(NH_3)_2Cl_2(OOCR)_2]$, where R = methyl, ethyl, propyl, butyl, pentyl, hexyl, heptyl, octyl, or nonyl, were all prepared in the same manner. Compound **1** (200 mg, 0.60 mmol) was suspended in 8 mL of DMF. To this mixture was added 1.5 mL of the appropriate carboxylic acid anhydride. The reaction mixture was stirred in the dark at 50 °C for 24 h. The resulting yellow to orange solution was filtered through Celite, and the volume of the filtrate was reduced to 2 mL in vacuo at 50 °C. This concentrated solution was then added in a dropwise manner to a rapidly stirring volume of diethyl ether (40 mL), forming a pale yellow to white precipitate. The ether suspension was stirred for 30 min, and the solid was collected by filtration and dried under a vacuum for 12 h. The detailed characterization of **2**–**10**, including spectroscopic and crystallographic data, is supplied in the Supporting Information.

Liquid Chromatography–Mass Spectrometry (LC–MS). Solutions (1:1 methanol/water containing 5% DMF) of **2**–**6** were injected onto an Eclipse XDB-C18 column (3 × 150 mm, Agilent) and eluted with 1:1 methanol/water at a rate of 0.25 mL/min. The elution was isocratic, and the temperature of the mobile phase within the column was maintained at 25 °C. The analytes were detected by monitoring the intensity of the negative ion mode base peak, which in all cases was the $[M - H]^-$ signal. The dead time of the column was evaluated by monitoring the elution of potassium iodide at 210 nm. This dead time was used in the calculation of the capacity factors of the analyzed Pt(IV) compounds.

Nanoparticle Encapsulation. A 550 μL DMF solution containing 10 mg of PLGA-PEG-COOH and an amount of the platinum complex to give the desired feed, defined as (mg of Pt complex/mg of polymer) × 100, was prepared. A 500 μL aliquot of this solution was added in a dropwise manner over the course of 10 min to 5 mL of rapidly stirring Milli-Q water. The DMF solutions were added by a mechanical pipet, and the nanoprecipitations were carried out in 20 mL glass scintillation vials. The water was stirred magnetically using a 0.5 cm stir bar at approximately 500 rpm. After addition of the DMF solution, the water acquired a milky blue coloration owing to Tyndall scattering of the nanoparticles that formed. At higher loadings, some macroscopic precipitation was also observed. An aqueous solution of poly(vinyl alcohol) (5 mL, 0.1% w/w PVA) was then added along the edge of the vial to bring the final volume to 10.5 mL and the final PVA concentration to approximately 0.05% w/w. This suspension of nanoparticles was stirred for an additional 20 min and then passed through a 0.45 μm cellulose acetate syringe filter (VWR). If macroscopic precipitation was evident, the suspension was first passed through a plug (0.25 × 1 cm) of Celite in order to avoid excessively clogging the syringe filter. The filtrate from the 0.45 μm filtration was loaded into an Amicon Centrifugal Filtration Device (100 kDa MWCO regenerated cellulose membrane). The loaded device was centrifuged at 1500*g* for 20 min, concentrating the nanoparticle suspension to approximately 1 mL. This concentrated material was suspended in an additional 10 mL of fresh Milli-Q water and centrifuged again under identical conditions. Each sample was washed three times in this manner. The final concentrated suspension was diluted to 1.4 mL with Milli-Q water for use in further experiments. All nanoprecipitations were carried out in triplicate.

Evaluation of Encapsulation. The metric used to evaluate encapsulation efficacy was the concentration of platinum present in the final 1.4 mL colloidal suspension. This concentration was determined by electrothermal atomic absorption spectroscopy (AAS) using a Perkin-Elmer AAnalyst 600 spectrometer outfitted with a transverse heated graphite atomizer. Platinum absorption was measured at 265.9 nm, and a Zeeman background absorption correction was applied. Samples were prepared by diluting nanoparticle suspensions with Milli-Q water until the platinum concentration fell within the linear calibration range (50–200 μg of Pt/L). All AAS measurements were carried out in triplicate and averaged.

Transmission Electron Microscopy. PLGA-PEG-COOH nanoparticles containing compound **10** at a 40% feed, the optimal loading conditions as described below, were prepared and an aliquot was allowed to evaporate on a carbon-coated copper TEM grid. Imaging was conducted by using a JEOL JEM-200CX operating at 120 kV.

RESULTS AND DISCUSSION

Synthesis. The nucleophilicity of hydroxo ligands coordinated to Pt(IV) centers provides a convenient synthetic route to Pt(IV) carboxylate compounds via condensation with an appropriate acid anhydride.[18] In the present work, this

dx.doi.org/10.1021/ic4010642 | *Inorg. Chem.* 2013, 52, 9915–9920

chemistry was carried out in DMF. As the reaction proceeds, the suspension of the dihydroxo compound **1** in DMF is consumed, forming a clear solution of the soluble dicarboxylatoplatinum(IV) product. The differential solubility of the starting material and product both drives the reaction and provides a convenient way to monitor its progress. To purify the compounds, the reaction volume was reduced in vacuo before addition to a large excess of diethyl ether. For many of the compounds, addition in the reverse order yielded only intractable oils. For longer chain carboxylates, the solubility of the products in DMF decreases. For example, **2**, with acetate ligands, is readily soluble at concentrations up to 100 mg/mL (0.24 M) at room temperature, but for **10**, which has decanoate ligands, a precipitate formed when a warm DMF solution of equivalent molar concentration was cooled to room temperature.

Physical characterization of the compounds confirmed their proposed structures. In the IR spectra of the products, sharp bands corresponding to O—H and Pt—O stretches in the starting material at 3516 and 559 cm^{-1}, respectively, are absent, and new bands in the ranges of 1665–1620 cm^{-1} (carbonyl C═O stretch), 1470–1190 cm^{-1} (C—H bend), and 2960–2850 cm^{-1} (C—H stretch) appear. The remaining notable features of the IR spectra are bands at 1530–1580 cm^{-1} (N—H bend) and 3260–3110 cm^{-1} (N—H stretch) that are present in both the starting material and the final products.

The ^{1}H NMR spectra of **2**–**10** all contain a resonance at approximately 6.52 ppm, consistent with protons on an ammine ligand bound to a Pt(IV) center. Features present on this signal arise from unresolved coupling of the protons to both ^{14}N and ^{195}Pt nuclei. For **2**–**5**, each additional methylene unit in the carboxylate chain produces a well-resolved resonance in the aliphatic region that displays the expected ^{1}H—^{1}H coupling pattern. As additional methylene groups are added from **6** to **10**, the overall CH_2 signal intensity increases, but individual units were not resolved at 500 MHz. The ^{13}C NMR spectra all display resolved peaks for the expected number of carbon atoms despite nearly overlapping signals (peak-to-peak separations of as little as 0.005 ppm) in some of the longer chains. The mass spectra all show the presence of the desired compound as indicated by $[M - H]^-$ peaks in negative ion mode ESI–MS.

Crystallography. The crystal structure of a DMSO solvate of *cis,cis,trans*-$[Pt(NH_3)_2Cl_2(OOCCH_3)_2]$, **2**·2DMSO, is depicted in Figure 1. Selected crystallographic parameters are presented in Table 1. Full details including bond lengths and angles are collected in Supporting Information Tables S1 and S3. The room temperature structure of a monohydrate of this compound has been previously reported.[19] In the previous structure, a 2-fold rotation axis passed through the platinum, but **2**·2DMSO has no such required symmetry. The orientations of the acetate ligands differ in the two structures, resulting in differing intramolecular hydrogen-bonding interactions, but the bond lengths and angles of the two are comparable. If allowances are made for flexibility of dihedral angles controlling the rotation of the acetate ligands, then the structures have a RMSD of 0.098 Å, as calculated with the program *MERCURY*.

The crystal structure of **3** was also determined. The apparent Laue symmetry visible in precession camera pseudoimages is 4/*mmm*, but no successful solution could be obtained in any of the space groups consistent with the 00*l*, $l \neq 4n$ systematically absent reflections. The abnormally low $\langle E^2 - 1 \rangle$ value of 0.525

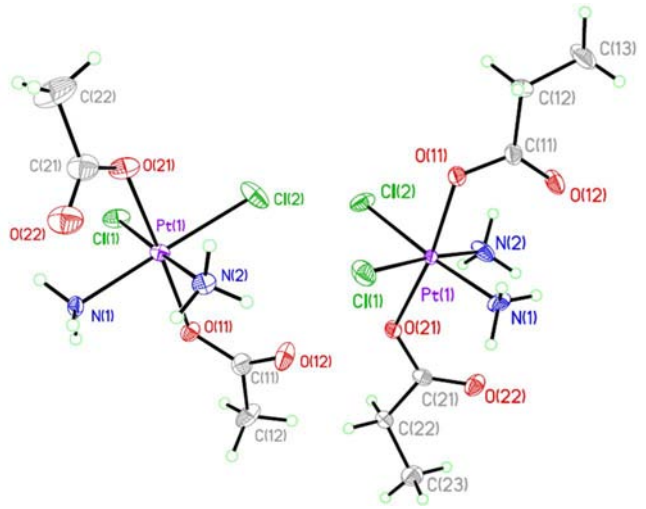

Figure 1. Molecular diagrams of **2** (left) and **3** (right). Thermal ellipsoids are drawn at the 50% probability level.

Table 1. Crystallographic Parameters for 2·2DMSO and 3

formula	$C_8H_{18}Cl_2N_2O_6PtS_2$	$C_6H_{16}Cl_2N_2O_4Pt$
formula weight	568.35	446.20
crystal system	triclinic	tetragonal
space group	$P\bar{1}$	$P4_3$
color	colorless	yellow
a, Å	7.2454(7)	9.2357(3)
b, Å	10.2263(10)	
c, Å	14.0657(14)	13.9563(11)
α, deg	72.516(2)	
β, deg	81.044(2)	
γ, deg	69.485(2)	
V, Å^3	929.51(16)	1190.45(11)
Z	2	4
T, K	100(2)	100(2)
$R_1{}^a$ (%)	3.42	1.68
$wR_2{}^b$ (%)	8.79	3.71
GOF^c	1.308	1.065

$^aR_1 = \sum||F_o| - |F_c||/\sum|F_o|$. $^bwR_2 = \{\sum[w(F_o^2 - F_c^2)^2]/\sum[w(F_o^2)^2]\}^{1/2}$. ^{c}GOF $= \{\sum[w(F_o^2 - F_c^2)^2]/(n-p)\}^{1/2}$, where *n* is the number of data and *p* is the number of refined parameters.

and the similarity between $R_{int}(4/mmm) = 0.093$ and $R_{int}(4/m) = 0.042$ suggested that the crystal may be twinned by merohedry. A Patterson map generated using preliminarily detwinned data revealed the locations of the Pt and Cl atoms. Subsequent refinement using the appropriate twin law afforded a satisfactory crystal structure (Figure 1). Selected crystallographic parameters are presented in Table 1. Full details including bond lengths and angles are collected in Supporting Information Tables S2 and S4.

Evaluation of Lipophilicity. The traditional measure of the lipophilicity of a molecule is the log of the water/octanol partition coefficient (log *P*).[20] Such values are typically obtained by the "shake-flask" method in which the analyte is introduced into a biphasic mixture of *n*-octanol-saturated water and water-saturated *n*-octanol. The compound is allowed to achieve a thermodynamic equilibrium between the two phases, and the concentration of analyte in each phase is determined. We find, however, that more reproducible results are obtained by using a reversed-phase high performance liquid chromatography (RP-HPLC) method.[21] For many compounds, including

dx.doi.org/10.1021/ic4010642 | *Inorg. Chem.* 2013, 52, 9915–9920

platinum complexes, the capacity factor under isocratic elution conditions is linearly proportional to log *P* values obtained by the shake-flask method.[22] Compounds **2**–**6** were analyzed by RP-HPLC and their capacity factors (*k*) are presented in Table 2. Chromatograms are shown in Supporting Information Figure S20.

Table 2. Retention Times and Capacity Factors of 2–6

compound	retention time (min)	capacity factor (*k*)
2	2.8	0.077
3	3.4	0.31
4	4.7	0.81
5	9.6	2.70
6	32.7	11.6

The lipophilicity of an organic molecule can be accurately modeled as the sum of the contributions from its individual functional groups.[23] When the log of the capacity factors of compounds **2**–**6** is plotted against the log *P* values of acetic through hexanoic acid, a straight line is obtained (Figure 2).

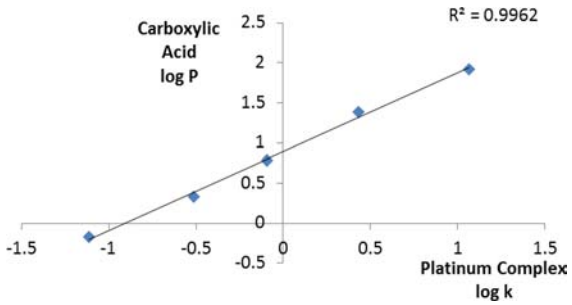

Figure 2. Correlation between the log of the capacity factors for **2**–**6** (abscissa) and the log of the octanol/water partition coefficients of the carboxylic acids from which the carboxylates of **2**–**6** are derived (ordinate).

This correlation indicates that the effect of adding additional methylene units to the carboxylate chain has approximately the same effect on the platinum complex as it does on the isolated carboxylic acid. Therefore, in subsequent analyses, we compare the properties of the platinum complexes with the log *P* values of the carboxylic acids from which the carboxylate ligands are derived.

Nanoparticle Encapsulation. The strategy used here to encapsulate compounds **2**–**10** within a polymeric nanoparticle has been successfully utilized to encapsulate other molecules.[12,17,24,25] The process by which the nanoconstruct forms is depicted schematically in Figure 3. An organic solution containing both an amphiphilic block copolymer and a potential guest molecule is added to a large excess of water. Provided that the organic solvent has been properly chosen so as to be readily miscible with water, this process drives self-assembly of the polymer chains into core–shell polymeric micelles. The hydrophobic block is buried within the core, and the hydrophilic block forms the solvent-exposed shell. When the polymer chains self-assemble, the additional hydrophobic guest molecule present in the initial organic solution can become trapped within the hydrophobic core of the particle.

The encapsulation of complexes **2**–**10** reflects the lipophilicities of their axial carboxylate ligands. Increasing the chain length increases the overall lipophilicity of the complex, facilitating its partition into the hydrophobic nanoparticle core. The series of platinum complexes reported here was prepared to determine the precise effect of chain length on the encapsulation of platinum complexes within a PLGA-PEG-COOH nanoparticle.

The specific experimental encapsulation procedure used was based upon a method described previously.[12] The polymer and platinum complex are dissolved together in DMF and added in a dropwise manner to a 10-fold excess volume of water. In previous studies using compound **6**,[9,10] acetonitrile was employed as the organic solvent, but not all of the compounds prepared here are sufficiently soluble in acetonitrile to allow for a unilateral comparison. When a droplet of the DMF solution comes into contact with the water, the organic solvent rapidly disperses into the aqueous phase, forcing the copolymer chains to assemble into micelles. In the process of nanoparticle

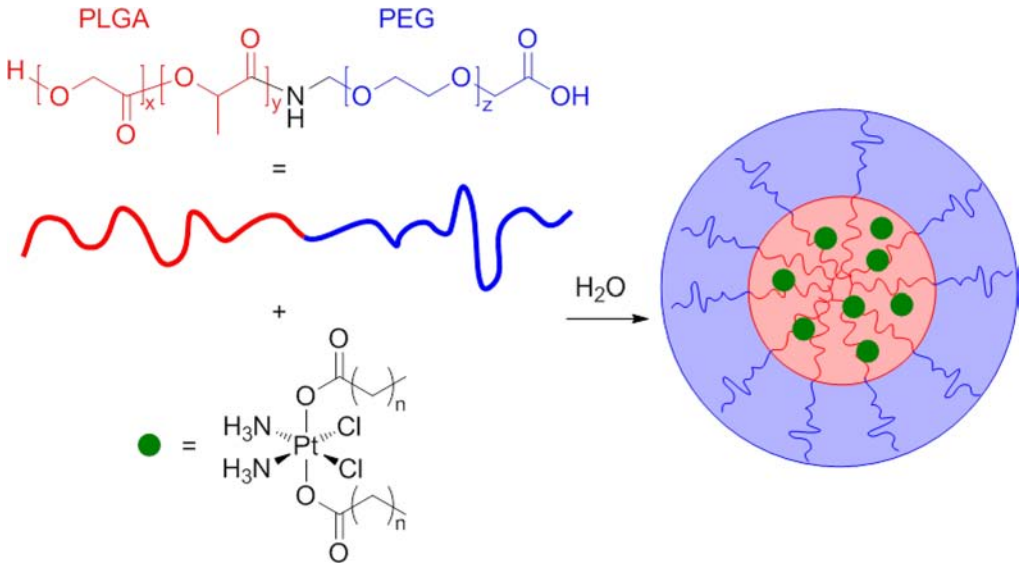

Figure 3. Schematic depiction of the nanoprecipitation process, whereby the amphiphilic block copolymer chains self-assemble into polymeric micelles, trapping hydrophobic guest molecules within.

dx.doi.org/10.1021/ic4010642 | *Inorg. Chem.* 2013, 52, 9915–9920

assembly, lipophilic platinum complexes that were present in the DMF solution are trapped within the hydrophobic core of the polymer nanoparticle.

During workup of the nanoparticle suspensions, particularly in the concentration steps using centrifugal filtration devices, the particles would often aggregate irreversibly. Inclusion of a small amount of a surfactant such as poly(vinyl alcohol) (PVA) during this stage of the preparation eliminated the problem.

When the encapsulation was carried out at a 10% feed—that is, when the platinum complex was present at 10% w/w with respect to the polymer in the DMF solution—a consistent trend was observed. As the chain length of the carboxylate ligand increased, the amount of the platinum complex encapsulated increased (Figure 4). Because log *P* of the

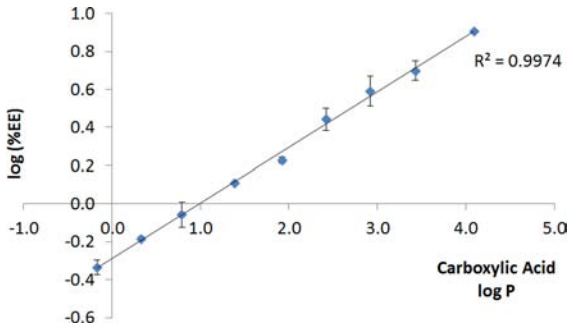

Figure 4. Correlation between the log of encapsulation efficiency (% EE) for **2**–**10** (ordinate) and the log *P* of the carboxylic acids from which the carboxylates of **2**–**10** are derived (abscissa).

carboxylic acid used as the ligand correlates with the lipophilicity of the entire platinum complex (vide supra), the log of the encapsulation efficiency (EE) was plotted against this parameter. The encapsulation efficiency is defined as the percent (w/w) of platinum complex encapsulated with respect to the amount used in the nanoprecipitation. Figure 4 shows that an excellent linear correlation exists between the aforementioned variables.

This correlation is intuitively satisfying, because one would expect that the platinum compounds should more readily encapsulate within the hydrophobic core of the nanoparticles as they become more lipophilic. Moreover, the linearity of the correlation attests to the reliability and reproducibility of the procedure.

Because **10** is the most effectively encapsulated at a 10% feed, it was selected to study the effect of feed variation on encapsulation. Initially, as the amount of platinum complex present during the nanoprecipitation was increased, the amount of platinum complex encapsulated increased as quantified by the loading, which is the percent (w/w) of platinum compound encapsulated with respect to polymer used in the nanoprecipitation (Figure 5). As the amount of platinum compound increased, however, the amount of macroscopic precipitation that occurred during nanoprecipitation also increased. This precipitation became so appreciable that samples had to be passed through a macroscopic filter aid prior to passage through 0.45 μm cellulose acetate membranes. This macroscopic precipitation also decreased the loading. The competing factors of increased loading and increased macroscopic precipitation resulted in a maximum loading when the feed was 40% (Figure 5).

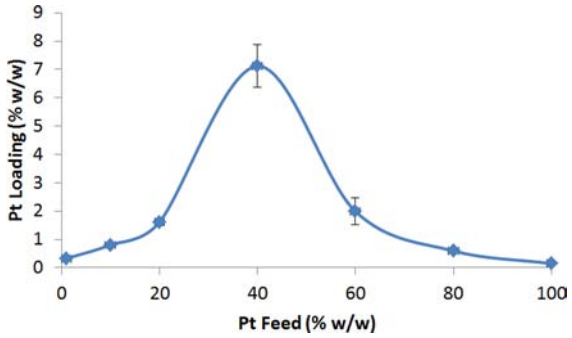

Figure 5. Variation in the platinum loaded into PLGA-PEG-COOH nanoparticles as the feed of **10** was varied.

Nanoparticle Characterization. Although a detailed examination of the effect of chain length of the Pt(IV) carboxylate complex on nanoparticle size and morphology was outside the scope of this study, measurements were made to confirm that the nanoparticles displayed characteristics consistent with the formulation provided above. The nanoparticles were imaged by TEM and the results are depicted in Figure 6. The nanoparticles appear as roughly circular black shapes, approximately 50 nm in diameter.

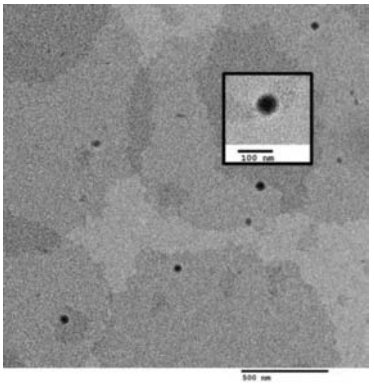

Figure 6. Transmission electron micrograph of PLGA-PEG-COOH nanoparticles loaded with **10**. Scale bar of main image = 500 nm, scale bar of inset = 100 nm.

CONCLUSION

This work presents a systematic investigation of the effect of ligand lipophilicity on the encapsulation of Pt(IV) prodrugs within PLGA-PEG-COOH nanoparticles. A procedure was optimized for encapsulation of a series of compounds spanning a wide range of lipophilicities. We find that, as the chain length increases, there is a direct and predictable increase in the degree to which the platinum complex is encapsulated. With the most readily encapsulated compound **10**, the effect of the platinum feed during nanoprecipitation was investigated. With an increase in concentration of platinum used in the nanoprecipitation, encapsulation also increased but so too did the amount of macroscopic precipitation. At higher feeds, macroscopic precipitation outweighed the increase in encapsulation. An intermediate feed level of 40% allowed for maximum loading of platinum complex **10** into the nanoparticles.

dx.doi.org/10.1021/ic4010642 | *Inorg. Chem.* 2013, 52, 9915–9920

■ ASSOCIATED CONTENT

Supporting Information

Spectroscopic and crystallographic characterization of **2**–**10**, detailed crystallographic parameters for the structure of **2**·2DMSO and **3**, selected bond lengths and angles of **2**·2DMSO and **3**, LC–MS chromatograms of **2**–**6**. Crystallographic information for **2**·2DMSO and **3** are also provided in CIF format. This material is available free of charge via the Internet at http://pubs.acs.org.

■ AUTHOR INFORMATION

Corresponding Author

*E-mail: lippard@mit.edu.

Notes

The authors declare no competing financial interest.

■ ACKNOWLEDGMENTS

This work was supported by grant CA034992 from the National Cancer Institute. Spectroscopic instrumentation at the MIT DCIF is maintained with funding from NIH Grant 1S10RR13886-01. T.C.J. received partial funding from the Harvard/MIT CCNE, NIH Grant 5-U54-CA151884. We acknowledge Dr. Suresh Gadde (Farokhzad lab, Harvard Medical School) for preparing the PLGA-PEG-COOH used in this study.

■ REFERENCES

(1) Rosenberg, B.; VanCamp, L.; Trosko, J. E.; Mansour, V. H. *Nature* **1969**, *222*, 385–386.
(2) Wheate, N. J.; Walker, S.; Craig, G. E.; Oun, R. *Dalton Trans.* **2010**, *39*, 8113–8127.
(3) O'Dwyer, P. J.; Stevenson, J. P.; Johnson, S. W. Clinical Status of Cisplatin, Carboplatin, and Other Platinum-Based Antitumor Drugs. In *Cisplatin - Chemistry and Biochemistry of a Leading Anticancer Drug*; Lippert, B., Ed.; Verlag Helvetica Chimica Acta: Zürich, Switzerland, 1999; pp 31–69.
(4) Kelland, L. *Nat. Rev. Cancer* **2007**, *7*, 573–584.
(5) Farokhzad, O. C.; Langer, R. *ACS Nano* **2009**, *3*, 16–20.
(6) Dhar, S.; Daniel, W. L.; Giljohann, D. A.; Mirkin, C. A.; Lippard, S. J. *J. Am. Chem. Soc.* **2009**, *131*, 14652–14653.
(7) Feazell, R. P.; Nakayama-Ratchford, N.; Dai, H.; Lippard, S. J. *J. Am. Chem. Soc.* **2007**, *129*, 8438–8439.
(8) Dhar, S.; Liu, Z.; Thomale, J.; Dai, H. J.; Lippard, S. J. *J. Am. Chem. Soc.* **2008**, *130*, 11467–11476.
(9) Dhar, S.; Gu, F. X.; Langer, R.; Farokhzad, O. C.; Lippard, S. J. *Proc. Natl. Acad. Sci. U. S. A.* **2008**, *105*, 17356–17361.
(10) Dhar, S.; Kolishetti, N.; Lippard, S. J.; Farokhzad, O. C. *Proc. Natl. Acad. Sci. U. S. A.* **2011**, *108*, 1850–1855.
(11) Kolishetti, N.; Dhar, S.; Valencia, P. M.; Lin, L. Q.; Karnik, R.; Lippard, S. J.; Langer, R.; Farokhzad, O. C. *Proc. Natl. Acad. Sci. U. S. A.* **2010**, *107*, 17939–17944.
(12) Cheng, J.; Teply, B. A.; Sherifi, I.; Sung, J.; Luther, G.; Gu, F. X.; Levy-Nissenbaum, E.; Radovic-Moreno, A. F.; Langer, R.; Farokhzad, O. C. *Biomaterials* **2007**, *28*, 869–876.
(13) Shamsuddin, S.; Santillan, C. C.; Stark, J. L.; Whitmire, K. H.; Siddik, Z. H.; Khokhar, A. R. *J. Inorg. Biochem.* **1998**, *71*, 29–35.
(14) Khan, S. R. A.; Huang, S.; Shamsuddin, S.; Inutsuka, S.; Whitmire, K. H.; Siddik, Z. H.; Khokhar, A. R. *Bioorg. Med. Chem.* **2000**, *8*, 515–521.
(15) Chen, F. M. F.; Kuroda, K.; Benoiton, N. L. *Synthesis* **1978**, 928–929.
(16) Hall, M. D.; Dillon, C. T.; Zhang, M.; Beale, P.; Cai, Z.; Lai, B.; Stampfl, A. P. J.; Hambley, T. W. *J. Biol. Inorg. Chem.* **2003**, *8*, 726–732.
(17) Farokhzad, O. C.; Cheng, J.; Teply, B. A.; Sherifi, I.; Jon, S.; Kantoff, P. W.; Richie, J. P.; Langer, R. *Proc. Natl. Acad. Sci. U. S. A.* **2006**, *103*, 6315–6320.
(18) Giandomenico, C. M.; Abrams, M. J.; Murrer, B. A.; Vollano, J. F.; Rheinheimer, M. I.; Wyer, S. B.; Bossard, G. E.; Higgins, J. D., III *Inorg. Chem.* **1995**, *34*, 1015–1021.
(19) Chen, L.; Lee, P. F.; Ranford, J. D.; Vittal, J. J.; Wong, S. Y. *J. Chem. Soc., Dalton Trans.* **1999**, 1209–1212.
(20) Leo, A.; Hansch, C.; Elkins, D. *Chem. Rev.* **1971**, *71*, 525–616.
(21) Harnisch, M.; Möckel, H. J.; Schulze, G. *J. Chromatogr.* **1983**, *282*, 315–332.
(22) Gramatica, P.; Papa, E.; Luini, M.; Monti, E.; Gariboldi, M. B.; Ravera, M.; Gabano, E.; Gaviglio, L.; Osella, D. *J. Biol. Inorg. Chem.* **2010**, *15*, 1157–1169.
(23) Hansch, C.; Fujita, T. *J. Am. Chem. Soc.* **1964**, *86*, 1616–1626.
(24) Farokhzad, O. C.; Jon, S. Y.; Khademhosseini, A.; Tran, T.-N. T.; LaVan, D. A.; Langer, R. *Cancer Res.* **2004**, *64*, 7668–7672.
(25) Fonseca, C.; Simões, S.; Gaspar, R. *J. Controlled Release* **2002**, *83*, 273–286.